The 8th International Conference on Jets, Wakes and Separated Flows, ICJWSF-2024
September 23-25, 2024, Firenze, Italy

Quantitative Flow Visualization of an Elliptic Underexpanded Sonic Jet by RST

T. Sakashita[1*], T. Nagata[1], S. Nakao[1], and Y. Miyazato[1]

1: Dept. of Mechanical Systems Engineering, The University of Kitakyushu, Japan

[*] Corresponding author: sakataku66@gmail.com

Abstract

Underexpanded jet issuing from an elliptic convergent nozzle with an aspect ratio of 8 is quantitatively visualized by rainbow schlieren tomography. The test nozzle has semi-major and semi-minor lengths of 10 mm and 1.25 mm, respectively, and an equivalent diameter of 7.1 mm. Flow visualization is performed at a nozzle pressure ratio of 4.0 to produce strong shocks in the jet plume. The Reynolds number based upon the equivalent diameter and flow properties at the nozzle exit is 4.0×10^5. Multi-view rainbow schlieren pictures with the horizontal filter setting are taken by rotating the nozzle around its central axis at an equal interval of 5° ranging from 0 to 180°. The jet density field is reconstructed using the convolution back projection method. The effects of image processing filters on the density fields including minor-axis and major-axis planes as well as the jet centerline and the liplines in the minor-axis and major-axis planes are examined. In addition, the flow features of a shock-containing elliptic jet are demonstrated.

Keywords: *Elliptic nozzle, Image processing, Rainbow schlieren tomography, Shock wave, Supersonic jet.*

1. Introduction

It has been widely recognized that elliptic nozzles have numerous advantages over conventional round and rectangular nozzles, such as improved flow mixing within the supersonic jet, shorter potential core length, enhanced shear layer entrainment and reduced shock-associated noise under certain operating conditions [1]. It suggests that elliptic nozzles are effective as a passive flow control strategy. Despite the engineering and academic importance of understanding the three-dimensional structures of shock-containing elliptic jets, little research has been done due to the lack of established measurement techniques.

Menon et al. [2] investigated the characteristics of underexpanded jets issuing from elliptic convergent nozzles with aspect ratios of 2 and 4 using shadowgraph technique and numerical simulations using the Reynolds-averaged Navier-Stokes (RANS) equations. Mitchell et al. [3] measured velocity fields in underexpanded jets issuing from an elliptic convergent nozzle with an aspect ratio (AR) of 2 using high-resolution planar particle image velocimetry (PIV) and displayed axis-switching phenomenon typical of asymmetric jet. Edington-Mitchell et al. [4] examined staging behaviour in screeching elliptic jets based on the frequency of the dominant screech tone. Nagata et al. [5] used rainbow schlieren deflectometry to visualize shock-containing jets emerging from an elliptic convergent nozzle with an aspect ratio of 2. They also proposed a flow model to analytically evaluate the effects of the nozzle pressure ratio and aspect ratio on the shock-cell spacing. Nagata et al.'s model [5] can quantitatively predict their experimental data and previous experimental values. Recently, Islam et al. [6] introduced an analytical model for shock-containing elliptic jets under slightly off-design conditions.

The primary objectives of this study are twofold. The first goal is to clarify the effects of image processing filters on the density field of the jet. The second goal is to reveal the flow features of the shock-containing jet emerging from an elliptic convergent nozzle with a high-aspect-ratio.

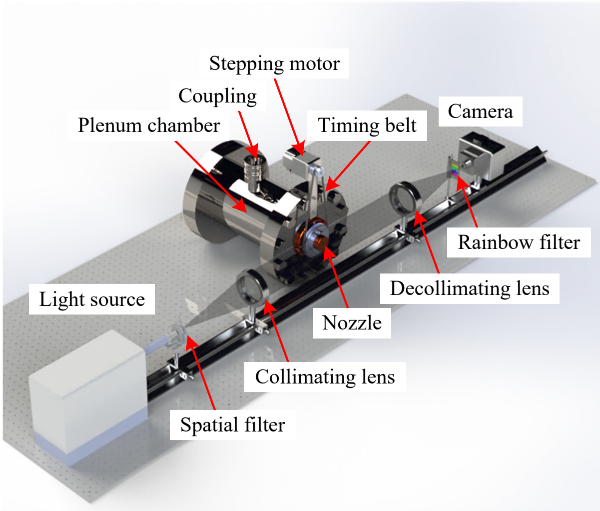

Fig. 1: Schematic diagram of the experimental apparatus with rainbow schlieren optical system

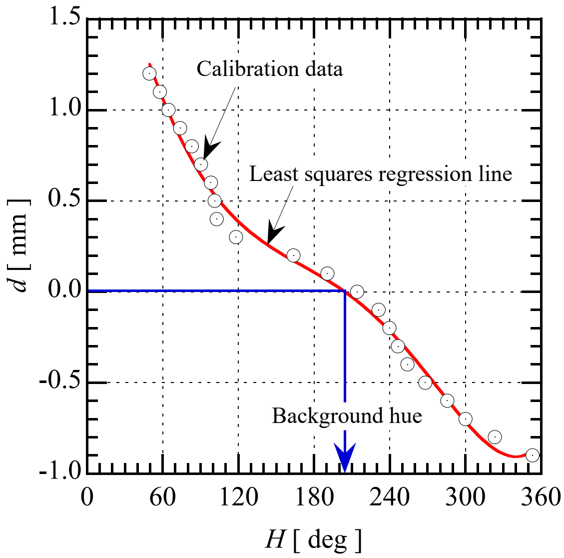

Fig. 2: Calibration curve of a rainbow filter

2. Experimental Methods

The experiments are conducted in an intermittent blowdown compressed-air facility [7]. Ambient air is pressurized by the compressor up to 1 MPa and stored in a high-pressure reservoir comprising two storage tanks with a total capacity of 2 m^3 after filtering and drying. An elliptic convergent nozzle with an aspect ratio (AR) of 8 at the nozzle exit is used as a test nozzle where the AR is defined as the ratio (L_a/L_b) of the semi-major length (L_a = 10 mm) to the semi-minor length (L_b = 1.25). The equivalent diameter [5] at the nozzle exit is given by $D_{eq} = 2(L_a L_b)^{1/2}$ and it becomes approximately 7.1 mm for the present nozzle. The Reynolds number, based upon the equivalent diameter and flow properties at the nozzle exit, is 4.01 $\times$ 10^5.

The high-pressure dry air from the reservoir is stagnated in the plenum chamber through a coupling as shown in Fig. 1. Subsequently, it is discharged into the quiescent air through the test nozzle that can be rotated about its central axis [7]. The desired nozzle pressure ratio (NPR = p_{os}/p_b) is achieved by changing the plenum pressure, p_{os}, with the back pressure, p_b, held constant at 4.0. In the present experiments, p_b is 101.8 kPa and the ambient temperature T_b is 299.8 K.

Quantitative flow visualizations of shock-containing elliptic jets are carried out by the rainbow schlieren tomography (RST) [7]. A rainbow filter is installed parallel to the flow in the cutoff plane of the schlieren. The filter is calibrated immediately before the experiment. The calibration curve of the rainbow filter used is shown in Fig. 2. The calibration curve is a fifth order least-squares approximation.

The jet density field of the jet is reconstructed by the convolution back projection (CBP) technique. Before the density field of the jet is reconstructed, three typical filtering processes including bilateral filter, block-matching and 3D (BM3D) filter, and total variation (TV) filter are applied to the rainbow schlieren image data.

3. Results and Discussion

3.1. Flow visualization

Rainbow schlieren pictures of a shock-containing elliptic jet are shown in Fig. 3 with flow flow left to right. To observe changes in the density gradient perpendicular to the flow direction, the rainbow filter is placed parallel to the flow in the schlieren cut-off plane. The color of the schlieren images corresponds to the hue value of the rainbow filter shown at the top of Fig. 3, and the magnitude of the density gradient is proportional to the difference from the background hue (204°). The hue values above the central axis of the jet exhibit lower values than the background hue as the density gradient increases, but higher values in the lower regions.

From Fig. 3, which shows the minor axis plane view, the jet exiting the nozzle initially spreads radially due to underexpansion, but contracts toward the location of the first shock just downstream of the nozzle to form the first shock cell. A second shock is faintly visible downstream of the first shock, but is obscured by the flow oscillations [8]. In Fig. 3, which shows the major-axis plane view, an incident shock can be seen to form a bow shape from the nozzle exit lip toward the center axis of the jet. A shock consisting of leading and rear shocks can be observed immediately after the bow shock. However, it is not possible to determine from this schlieren image whether a Mach stem is formed on the central axis of the jet. The jet boundary in the major-axis plane view gradually decreases in the downstream direction toward the jet centerline from just after the nozzle exit. It should be kept in mind that the rainbow schlieren images in Fig. 3 demonstrate the result of averaging the density gradient perpendicular to the jet axis in the viewing direction.

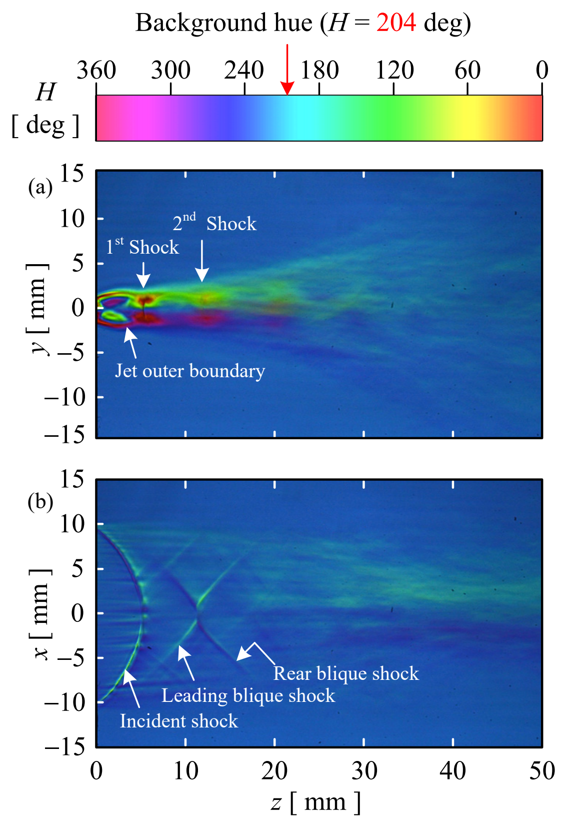

Fig. 3: Rainbow schlieren pictures of the elliptic underexpanded jet taken with the horizontal rainbow filter setting where (a) minor-axis plane view and (b) major-axis plane view

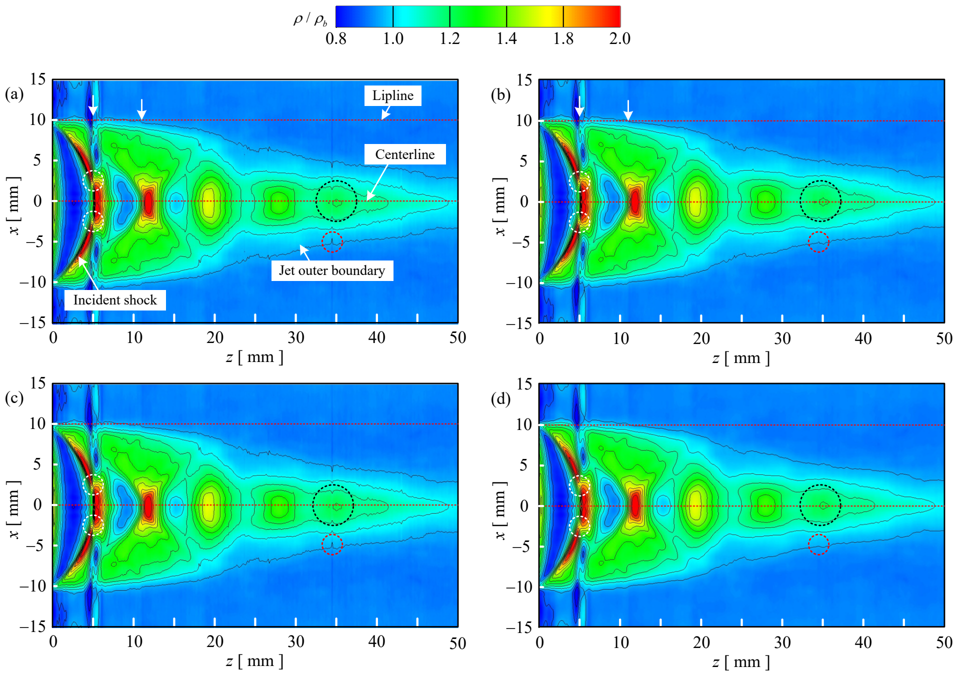

Fig. 4: Density contour plots of the elliptic underexpanded jet with (a) no filter, (b) bilateral filter, (c) block-matching and 3D (BM3D) filter, and total variation (TV) filter

3.2. Density contour plots

The density contour plot of an underexpanded jet issuing from an elliptic convergent nozzle of AR = 8 at NPR = 4.0 is shown in Fig. 4 with the flow from left to right. The density field is normalized by the ambient density (ρ_b). The origin of the coordinate system is the center of the cross section at the nozzle exit. The abscissa and ordinate denote the streamwise distance (z) and the horizontal distance (x) along the major-axis from the origin, respectively. The contour level is represented by a color bar at the top of Fig. 1 as a range from a minimum value of 0.8 to a maximum value of 2.0. The red dashed lines parallel to the abscissa indicate the centerline (x = 0 mm) and lipline (x = 10 mm). The white downward arrows denote the shock locations at the centerline. Figure 4(a) is the original density field without image processing. An arc-shaped shock can be observed originating from the nozzle exit lip and extending toward the central axis of the jet, but it forms a discontinuity near the central axis of the jet, as shown by the two white circles. A short X-shaped shock surrounded by a butterfly-shaped isopycnic line can be clearly observed as the second shock. The width between the upper and lower jet outer boundaries decreases slowly in the flow direction from the nozzle exit, but decreases abruptly at z = 20 mm and then rises slightly. Thereafter, it gradually decreases in the downstream direction. In previous studies [2, 3] using elliptic convergent nozzles of AR= 2 at NPR= 4, the first shock in the major-axis plane is a Mach shock consisting of an incident shock, a reflected shock, and a Mach stem, forming a distinct slip line. However a Mach stem with a slipline can not be recognized in Fig. 2(a). The two discontinuities of the arc-shaped shock at z = approximately 5 mm are not a physical phenomenon, but noise. The spike-like abrupt change that appears in the isopycnic lines at z = 34 mm also indicates the effect of noise. The outer isopycnic line, indicating the jet outer boundary, is found to contain noise at z greater than approximately 22 mm.

Figures 4(b)$\sim$(d) are the density fields with image processing by bilateral filter, block-matching and 3d (BM3D) filter, and total variation (TV) filter, respectively. The bilateral filter is a non-linear, edge-preserving, and noise-reducing smoothing filter for images and it preserves sharp edges. The BM3D filter is a 3-D block-matching algorithm used primarily for noise reduction in images. The TV filter is based on the principle that signals with excessive and possibly spurious detail have a high total variation. Focusing on the areas circled by the red and blue dashed lines, one can see that the TV filter removes noise the best. It can be seen that all filters fail to eliminate the discontinuous noises in the areas circled by the white dashed lines at z = 5 mm and the bilateral and TV filters succeed in removing noises at z = 34 mm.

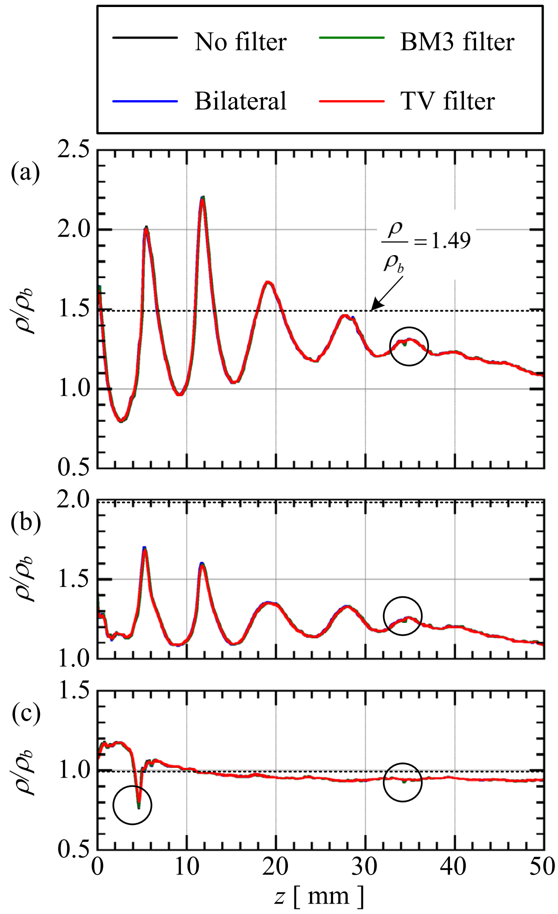

Fig. 5: Streamwise density profiles along the (a) jet centerline, (b) lipline in the minor-axis plane, and (c) major-axis plane where the black line denotes no filter, blue the BM3D filter, green the bilateral filter, and red the TV filter

3.3. Streamwise density distributions

Typical density distributions along (a) jet centerline, (b) lipline in the minor-axis plane, and (c) lipline in the major-axis plane are shown in Fig. 5. The vertical axis denotes the density normalized by the ambient density and horizontal axis is the streamwise distance from the nozzle exit. The dashed line parallel to the horizontal axis in Fig. 5 shows the normalized density at the jet-free boundary, where the static pressure is the same as the back pressure, but the density is different from the ambient density. The solid red line in Fig. 5 shows the results with the TV filter applied, but actually includes the results with the BM3 and Bilateral filters as well as the unfiltered result. However, the effect of the filters on the density distribution is negligible, and the differences appear only in the circled areas in Figs. 5(a), (b) and (c).

From Fig. 5, the effect of the image processing filters on the density distribution in the flow direction is negligible, so we discuss the details of the jet structure by focusing only on the density distribution with respect to the TV filter. The theoretical density ratio at the nozzle exit is about 2.5 compared to the experimental value of about 1.7. This is probably due to the reflection of light at the nozzle exit cross section. At 2 mm downstream of the nozzle exit, the density in the jet rapidly decreases to 80% of the atmospheric density, and the theoretical Mach number at this position is predicted to be about 2.1, assuming an isentropic change.

The maximum Mach number in underexpanded jets emerging from a convergent nozzle is predicted to occur at the first minimum of the density or static pressure distribution on the jet central axis. For reference, Tashiro et al. [9] proposed an experimental relation

$$M = 1 + 0.72\,(\mathrm{NPR} - 1.89)^{0.76} \tag{1}$$

for the Mach number obtained from the first minimum value of the density profile along the central axis of underexpanded jets issuing from a circular convergent nozzle. Substituting NPR = 4 into Eq. (1) gives a

Mach number of approximately 2.3. The effects of AR and NPR on the maximum Mach number inside the shock-containing elliptic jets are left for future research.

In the density distribution along the jet centerline as shown in Fig. 5(a), the streamwise locations of the local density maxima correspond approximately to those of the shocks. The values of the local density maxima are largest at the location of the second shock, which is attributed to the strength of the shock. In addition, the distance between the streamwise locations of the first and second density maxima indicates the shock-cell length [5]. The shock-cell length normalized by the equivalent diameter can be obtained as 0.88 from the density profile along the jet centerline in Fig. 5(a). This value is almost equal to the analytical value of 0.93 predicted using the previous flow model [5].

4. Conclusions

An underexpanded jet issuing from an elliptic convergent nozzle with AR = 8 was experimentally investigated by rainbow schlieren tomography. Three representative image processing filters, including Bilateral, BM3D and TV were applied to the rainbow schlieren images to reconstruct the three-dimensional density field of the jet. The conclusions obtained are as follows.

(1) Of the three image processing filters used, the TV filter is the best at removing noise in the density fields of shock-containing jets. However, the filters have little effect on the three typical density distributions along the jet's central axis, the lipline in the minor axis plane, and the lipline in the major axis plane.

(2) In the minor-axis plane, an elliptic underexpanded jet forms the first shock-cell by slightly expanding the jet boundary in the radial direction immediately after the nozzle exit and then contracting toward the location where the first shock is generated. After the first shock-cell, the jet boundary expands sharply in the radial direction. On the other hand, in the major-axis plane, the jet boundary just after the nozzle exit shrinks toward the central axis of the jet with increasing streamwise distance.

(3) In the density distribution on the central axis of the jet, the second local maximum is the largest among all local maxima. In addition, the shock-cell length, normalized to the equivalent diameter, is 0.88 for the present experiment. It is close to the analytical value, 0.93, predicted by the flow model proposed by Nagata et al.

Acknowledgments

The authors thank Dr. Takeshi Miyakuni of the University of Kitakyushu for fabricating the elliptic convergent nozzle used in the experiment. This work was supported in part by Institute of Environmental Science and Technology, The University of Kitakyushu.

References

[1] Kinzie K. and McLaughlin D. K. "Aeroacoustic Properties of Supersonic Elliptic Jets". In: *Journal of Fluid Mechanics* 395 (1999), pp. 1–28.

[2] Menon N. and Skews B. W. "Shock Wave Configurations and Flow Structures in Non-Axisymmetric Underexpanded Sonic Jets". In: *Shock Waves* 20 (2010), pp. 175–190.

[3] Mitchell D. M. et al. "Near-Field Structure of Underexpanded Elliptic Jets". In: *Experiments in Fluids* 54 (2013), p. 1578.

[4] Edgington-Mitchell D. et al. "Staging Behavior in Screeching Elliptical Jets". In: *International Journal of Aeroacoustics* 14 (7) (2015), pp. 1005–1024.

[5] Nagata T. et al. "Shock-Cell Spacings of Underexpanded Sonic Jets Emerging from Elliptic Nozzles". In: *Experiments in Fluids* 63 (7) (2022), p. 111.

[6] Islam M. M. et al. "Theoretical Study of Slightly Underexpanded Jets from Elliptical Nozzles". In: *Transactions of the Japan Society for Aeronautical and Space Sciences* 67 (1) (2024), pp. 32–39.

[7] Fukunaga R. et al. "Application of Rainbow Schlieren Tomography for Shock-Containing Rectangular Jets". In: *Journal of Visualization* 25 (4) (2022), pp. 687–695.

[8] Edgington-Mitchell D. "Aeroacoustic Resonance and Self-Excitation in Screeching and Impinging Supersonic Jets - A Review". In: *International Journal of Aeroacoustics* 18 (2-3) (2019), pp. 118–188.

[9] Tashiro T. et al. "Flow Features of Underexpanded Microjets Emerging from a Round Convergent Nozzle". In: *Experiments in Fluids* 64 (3) (2023), p. 55.